ec r
u t s

Bar-Built Estuary Breach Detection with Remote Sensing: an Automated Tool to Inform Management Practices

Sarah A. R. Payne[1,2] · Karina Alvarez[1,3] · Molly Bruce[1,4] · Rachel Darling[1,5] · Alex Gunnerson[1] · Roger Ly[1] · Sophia Stonebrook[1] · Erica Carcelen[6] · Benjamin Holt[7] · Bruce Chapman[7] · Christine Lee[7]

Received: 22 July 2024 / Revised: 17 March 2025 / Accepted: 20 April 2025

Abstract

Bar-built estuaries (BBEs) are dynamic habitats that are subject to a number of natural factors (precipitation, tidal influence, sediment transport, etc.) and anthropogenic factors (run-off, managed breaches, etc.) that influence their environmental state. While informed management requires an understanding of these factors and their seasonal patterns, documenting estuary conditions is challenging due to a limited capacity for in situ monitoring. To better understand seasonal changes in estuaries, this research used satellite remote sensing to examine estuary mouth state and inundation extent. We used Sentinel-2 MultiSpectral Instrument (MSI) and Sentinel-1 C-band Synthetic Aperture Radar (C-SAR) to develop the California Estuary Assessment (CEA) tool in Google Earth Engine. The Sentinel-1 C-SAR and the Sentinel-2 MSI-derived Normalized Difference Water Index captured the estuary mouth state, in terms of opened or closed, and inundation extent. We then compared the estuary mouth state and inundation extent seasonally. The Navarro River Estuary exhibited much more frequent closed mouth state observations (70% of all observations) compared to the Russian River (26% of all observations). Inundation patterns also varied between the estuaries and between seasons—at Navarro River, the lowest and highest inundation values occurred in summer (71.5% of maximum inundation extent) and spring (75.8%), respectively, while at Russian River, the lowest and highest values occurred in summer (68.3%) and fall (86.2%), respectively. Furthermore, inundation extent varied significantly more in fall at Navarro River, and in spring and summer at the Russian River. Our findings reveal substantial seasonal differences between BBEs that highlight the importance of monitoring individual systems.

Keywords Bar-built estuaries · Breach state · NDWI · Remote sensing · Estuary mouth state · Seasonality

Introduction

Approximately half of California's 577 coastal confluences, areas where freshwater meets the ocean, are bar-built estuaries (BBEs) that are periodically closed to the tides (Clark & O'Connor, 2019). These types of estuaries, also known as intermittently closed estuaries, have complex dynamics governing their opening and closure. Sandbars fail in BBEs, opening the estuary mouth, through an increase in

Communicated by Paul A. Montagna

Sarah A. R. Payne and Karina Alvarez contributed equally to this work and shared first authorship.

Erica Carcelen, Benjamin Holt, Bruce Chapman, and Christine Lee share senior authorship.

✉ Sarah A. R. Payne
sarahallisonrose@gmail.com

[1] NASA DEVELOP, Langley Research Center, Hampton, VA, USA

[2] University of California, Santa Barbara, Santa Barbara, CA, USA

[3] University of Wuerzburg, Wuerzburg, Germany

[4] Center for Law, Energy and the Environment, Berkeley, School of Law, University of California, Berkeley, CA, USA

[5] Sea Grant, University of Southern California, Los Angeles, CA, USA

[6] Science Systems and Applications, Inc., Lanham, MD, USA

[7] Jet Propulsion Laboratory, California Institute of Technology, Pasadena, CA, USA

Published online: 25 May 2025

groundwater, precipitation, and river discharge (Clark et al., 2013; Rich & Keller, 2013). During river discharge events, lagoon water levels can be higher than ocean surface levels creating a pressure gradient that is directed offshore, meaning that water is driven to flow from the estuary into the ocean. However, this gradient is balanced by wave and tidal energy, therefore creating complex BBE patterns of opening and closure (Orescanin & Scooler, 2018; Orescanin et al., 2021). Depending on the inlet size, morphology, tidal currents, and inundation of the estuary, wave energy in particular can play a large role in BBEs opening and closure. High wave energy comes from storms or strong tidal cycles and can either open the estuary mouth with wave action that degrades sandbars or form sandbars that close the estuary mouth (Bertin et al., 2019; Rich & Keller, 2013). On a non-BBE coastline, wave energy can reflect or dissipate, while estuaries can be conducive to receiving tidal energy that propagates within the estuarine system (Bertin & Olabarrieta, 2016). When BBEs are closed, estuaries receive only freshwater input except during large wave events and bidirectional seepage through the sandbar; in contrast, during a breach event, tidal influences impact the estuary (Clark & O'Connor, 2019).

Seasonal trends of precipitation and wave action influence patterns of BBE opening and closure. California's Mediterranean climate leads to hot, dry summers and wet winters that result in highly variable, episodic stream flow (Behrens et al., 2013). Previous literature on California BBEs has found that water level fluctuations, breach events, and maximum inundation extent tend to occur most in spring and late fall due to fluvial discharge and wave overtopping events, respectively. In contrast, inundation extent and mouth state are fairly stable in summer (Clark & O'Connor 2019). In addition to seasonal stream discharge, these regions experience increased wave energy in winter compared to summer (Harris et al., 2002). These patterns may be particularly important for small inlets where the closure pattern is primarily governed by the seasonal cycles in wave height and river flow, while at the interannual scale, closures are more strongly related to river flow (Behrens et al., 2009; Orescanin et al., 2021). Alongside seasonal variability, variability among years (e.g., due to El Niño Southern Oscillation pattern) and among systems (e.g., due to size, hydrology) is substantial (Largier et al., 2019).

BBEs' sandbar formation and failure create unique systems that provide a multitude of ecosystem services. BBEs contain robust and diverse habitats (Clark & O'Connor, 2019; Dawson et al., 2023) that provide numerous ecological functions such as filtering pollutants out of the water, providing a protective habitat for endangered and threatened species, and acting as nurseries for fish and invertebrates (Barbier et al., 2013). Additionally, BBEs, like other estuaries, buffer coastal hazards such as storm surge, protecting structures behind them from flooding. Unlike permanently closed estuaries, BBEs are more likely to keep pace with rising sea levels precisely because of their intermittent closures, making them particularly resilient to climate change (Thorne et al., 2021).

Despite their environmental importance, BBEs, especially those in heavily urbanized environments, are subject to a variety of anthropogenic activities that disrupt the timing, magnitude, and duration of estuarine processes (Dahl, 1990; Heady et al., 2015; Largier et al., 2019). For example, BBEs can pose a flood risk to adjacent development during closures as water accumulates behind the sandbar. In these cases, artificially managed breaching is a common flood management practice (Behrens et al., 2013; Ranasinghe & Pattiaratchi, 2003; Stretch & Parkinson, 2006). Managed breaches are also used to allow passage of anadromous fish species during spawning season (Goodwin & Cuffe, 1994). Analyzing the natural opening and closure patterns of these systems will assist managers in their understanding of managed breaches' impact on wildlife, flood protection, and other valuable ecosystem services.

To support the management of such systems, the California Legislature enacted the Marine Life Protection Act (MLPA) in 1999. The MLPA includes protection for estuaries and estuarine ecosystem services (among other coastal systems) such as estuary function, structure, diversity, cultural value, and educational value. Crucially, the MLPA requires consistent monitoring of California's network of Marine Protected Areas (MPAs; Kirlin et al., 2013), which include some BBEs. However, in situ data monitoring—the historical means by which these ecosystems were monitored—is time-intensive, physically demanding, and expensive, thereby limiting resource managers' capacity to engage in consistent and robust monitoring across all of California's estuarine MPAs. Furthermore, for those MPAs that are well monitored, there is a deficiency of sequential, historical data upon which California's resource managers can utilize to understand estuaries and protect them from anthropogenic impact.

While efforts to model and understand BBE closure and opening dynamics have advanced (Behrens et al., 2013; Rich & Keller, 2013; Orescanin & Scooler, 2018; Orescanin et al., 2021), further research on the link between various conditions, such as El Niño Southern Oscillation (ENSO), and closure pattern is still needed (Thorne et al., 2021). By accessing historical closure data, researchers and managers can overlay these data with in situ data (such as ENSO condition, tide, and storm surge) to better understand dynamics and inform inferential models. Publicly available remotely sensed satellite data can provide a more cost and time-efficient way to gather information on California estuaries, especially

when in situ monitoring is impractical. Remotely sensed data also allows managers to complete long-term, retrospective analyses at high temporal and spatial resolution. A high temporal resolution is essential because opening and closure of the BBEs, and associated changes in inundation, can occur rapidly, on the scale of hours. Similarly, high spatial resolution is essential as estuary mouth openings may be small, less than 10 meters (m), and vegetation surrounding the estuary may "hide" water underneath if the pixel size is too large. Combining multiple satellite sensors offers an opportunity to provide the temporal and spatial resolution required to better understand these estuary systems.

The objective of this research is to utilize remote sensing to help California estuary managers better understand historical and current estuary mouth state patterns and associated inundation extent seasonally. To do this, the study team created the California Estuary Assessment (CEA) tool in Google Earth Engine (GEE). This analysis utilizes remotely sensed satellite imagery from Sentinel-2 MultiSpectral Instrument (MSI), Sentinel-1 C-band Synthetic Aperture Radar (C-SAR), and PlanetScope multispectral sensor data. The satellites and their respective sensors measure surface reflectance and backscatter intensity to examine estuary mouth state and inundation from December 2018 to July 2021. The CEA tool outperforms alternative remote sensing breach detection methods and successfully captures mouth state and inundation based on its novel method and use of recently available satellite data. This information can be used to better inform and potentially forecast management needs under changing climatic conditions. In this paper, we use the CEA tool to investigate the seasonal variability of mouth state and inundation extent. We hypothesized that the number of open mouth state observations will be highest in winter and early spring due to increased river discharge and increased wave activity (Behrens et al., 2013, Clark & O'Connor 2019), and as a result, inundation extent will be more variable. Additionally, we hypothesized that in the summer, BBEs will have fewer changes in mouth state and inundation due to lower amounts of river discharge and reduced wave action.

Methods

Data Acquisition

We acquired satellite imagery from Sentinel-2 MultiSpectral Instrument (MSI) and Sentinel-1 C-Synthetic Aperture Radar (C-SAR) through the Google Earth Engine catalog (Gorelick et al., 2017) and obtained PlanetScope data through Planet Explorer (Planet Team, 2017, Table 1).

As referenced in Table 1, satellites have different temporal resolutions—how long it takes for the satellite to return to the same location. Temporal resolution is displayed by the number of days as the specific time each day may vary due to ascending and descending orbits. Satellites also have different spatial resolutions—the area of ground represented by a single pixel. Satellite sensors collect data as bands, where each band represents a certain wavelength of light that reaches the sensor (Xu, 2006).

Sentinel-2 MSI data are collected by twin satellites, Sentinel-2A and Sentinel-2B, in a sun-synchronous polar orbit allowing for a temporal resolution of approximately every 5 days. The MSI collects data in bands covering the visible to short wave infrared portion of the electromagnetic spectrum as radiation values (Elachi & van Zyl, 2006; Gonenc et al., 2019). Therefore, when the natural radiation is hindered, for example by clouds, the instrument is not able to capture an accurate ground image. The specific image collection for Sentinel-2 MSI in GEE is Level 2A Surface Reflectance data which means there is robust atmospheric correction alongside scene classification (such as identifying clouds and cloud shadows) that allows for further refinement of the data through cloud masks and cloud filters discussed in later sections (Copernicus Sentinel-2 MSI Level- 2A Data, n.d.). While Sentinel-2 MSI has 13 bands at different spatial resolutions, the researchers only used data at a 10 m spatial resolution (bands of light representing red, green, blue, and near-infrared) to analyze the estuary mouth state and inundation extent. The 60 m quality assurance (QA60) band was also used to identify cloudy images.

Sentinel-1 C-SAR data are also captured by two satellites, Sentinel-1A and Sentinel-1B, in a polar orbit that captures data both day and night and has a temporal resolution of 2 to

Table 1 Earth observation data acquired for Sentinel-2 MSI, Sentinel-1 C-SAR, and PlanetScope imagery

Platform and sensor	Processing level	Spatial resolution	Spectral resolution	Date range of available data	Source	Use
Sentinel-2 MSI	Level 2A SR	10,20, 60 m, ~ 5 day revisit	13 bands	December 2018 to present	ESA	Surface reflectance
Sentinel-1 C-SAR	Level 1 GRD	10 m, ~ 2–3 day revisit	5.405 GHz (HH, HV, VV, VH)	April 2014 to present	ESA	Backscatter intensity
PlanetScope	Level 3A	3 m, ~ 1–2 day revisit	4 bands	June 2016 to present	Planet Labs	Surface reflectance

3 days, depending on the latitude of study. Sentinel-1 C-SAR uses active remote sensing, distinct from the passive sensing of Sentinel-2 MSI. Sentinel-1 C-SAR uses a single band, the C-band microwave region of the electromagnetic spectrum at 5.405 Gigahertz. An active sensor produces its own energy and then records the amount of that energy reflected back after interacting with the Earth's surfaces, which is known as backscatter (Elachi & van Zyl, 2006). C-SAR imagery has a longer wavelength compared to optical, allowing it to pass through clouds undisturbed to capture areas of interest (Copernicus Sentinel-1 C-SAR Level 1 Data, n.d.). This allows for a higher temporal frequency of data collection as atmospheric interference or sunlight is not a concern. Given the different but complementary traits of C-SAR imagery, the researchers used this data at a 10 m spatial resolution to augment inundation measurements using optical sensors.

PlanetScope data are collected from a constellation of over 130 sun-synchronous satellites with a temporal resolution of every 1 to 2 days. This commercial sensor is also passive, and therefore, as with Sentinel-2 MSI, when the natural radiation is hindered, for example by clouds, the satellite is not able to capture an accurate ground image. The PlanetScope sensor is a multispectral instrument that captures four bands of light ranging from the visible to near-infrared portion of the electromagnetic spectrum. The sensor has a high spatial resolution of approximately 3 m (Planet Team, 2017). PlanetScope's high temporal and spatial resolution made it an appropriate dataset to verify the CEA tool's estuary mouth state analysis and visually inspect inundation levels.

Ultimately, we used GEE to access satellite sensor data from Sentinel-2 MSI and Sentinel-1 C-SAR and create the CEA tool. We then used PlanetScope's high temporal and spatial resolution data to determine the accuracy of our tool. The CEA tool combines imagery from Sentinel-2 MSI and Sentinel-1 C-SAR satellite sensors to create a comprehensive visual package to understand estuarine dynamics.

Ancillary datasets used in this study included the United States Fish and Wildlife Service (USFWS, 2018) National Wetlands Inventory (NWI), United States Geological Survey (USGS, 2019) 3D Elevation Project (USGS 3DEP) 1 m Digital Elevation Models (DEMs), and NOAA Coastal National Elevation Database (CoNED, n.d.) 1 m DEMs. NOAA CoNED DEMS represent a compilation of topography and bathymetry data collected from 1986 to 2020. We used these datasets to designate the five estuary study areas used in the CEA tool. Water level data from Navarro (December 2018 through August 2020) and Russian River (December 2018 through June 2021) estuaries, courtesy of the Moss Landing Marine Laboratories Coast Wetlands Group and Sonoma Water respectively, were used to further validate the tool.

Software

The primary software we used was the GEE JavaScript API accessed through the web-based integrated development environment, Earth Engine Code Editor. The GEE JavaScript API was used to access imagery and create the CEA tool. We used Esri ArcMap 10.7.1 to create the estuary mouth state and inundation shapefiles and QGIS 3.28.3 to create a hypsometric curve based on acquired digital elevation models. Finally, Python 2.7 was used to assess the accuracy of the CEA tool in comparison to InletTracker, and RStudio 2023.09.0 + 463 was used to assess seasonal differences of estuary characteristics.

Study Area Selection

This study focuses on five of California's numerous estuaries: Navarro River Estuary, Russian River Estuary, Carmel River Estuary, Malibu Lagoon, and Ventura River Estuary, three of which are MPAs (Navarro, Russian, and Carmel; Fig. 1). These five estuaries were selected primarily based on their size and location. The team selected estuaries that were large enough that changes could be detected by satellite sensors but that were not so large that the estuary's mouth never closed or where changes were concealed by the sheer scale of the system. The team also sought to work with estuaries that spanned California's entire coastline rather than focus on only one region of the state. Testing larger and smaller sites allowed the researchers to determine the spatial resolution limits of the CEA tool. Some of these estuaries were also selected because there was existing in situ data to which the team could compare its findings. For estuaries with the highest mouth detection accuracy, Russian River and Navarro, further analysis explored the relationship of remotely sensed mouth state to inundation and the estuary's seasonal patterns.

Defining Estuary Boundaries

This project generated two shapefiles in ArcMap 10.7.1 specifically suited to detecting estuary mouth state and estuary inundation extent separately. To create the estuary inundation shapefile (Fig. 1), we overlapped the USFWS NWI shapefile and a DEM clipped to include only areas under 5 m in elevation. Depending on data availability for the site, we used either a USGS 3DEP 1 m DEM or NOAAs CoNED 1 m DEM. We then clipped the shapefile to include only the landward side of the estuary. To create the estuary mouth state shapefile, the researchers visually inspected the imagery to see where breaches often occurred and placed a

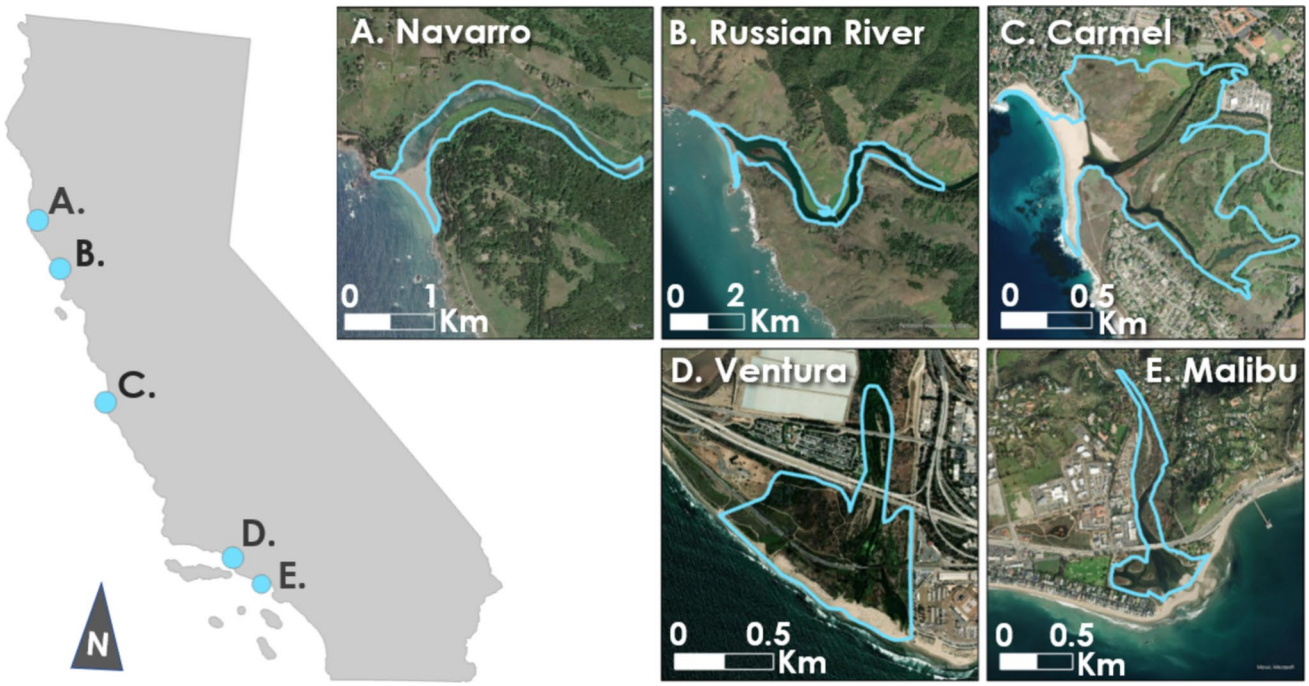

Fig. 1 The five selected estuary study sites and associated image examples using ArcMap 10.7.1 Esri base map. The five estuary inundation study areas are displayed in blue outline. The estuary mouth points' latitude and longitude are **A** Navarro Mouth (39.190814°N, −123.760179°W), **B** Russian River Mouth (38.449689°N, −123.128217°W), **C** Carmel Mouth (36.537513°N, −121.928230°W), **D** Ventura Mouth (34.274826°N, −119.308674°W), and **E** Malibu Mouth (34.033046°N, −118.680511°W)

point at the center of the estuary mouth. We then created a 500 m buffer around this point for all sites except Malibu, where a 250 m buffer was used due to the estuary's small mouth. We intersected the buffer with the inundation polygon and excluded areas identified as land. This produced an estuary mouth state polygon with areas extending from the seaward side and landward side of the estuary mouth. We then uploaded the estuary mouth state polygon and inundation polygon as assets to GEE.

Estuary Mouth State Detection

In GEE, we detected the estuary mouth state by assessing the continuity of water pixels between the estuary and open ocean using Sentinel-2 MSI imagery (Fig. 2A). To ensure clear optical imagery, we applied two cloud filters. The first cloud filter removed any image with greater than 20% cloud cover in the entire Sentinel-2 MSI image based on the image metadata. The researchers applied a second cloud filter based on the Sentinel-2 MSI QA60 band. The QA60 band is a quality assurance band provided at a 60 m resolution that identifies dense clouds or cirrus clouds based on a pixel's reflectance. If the QA60 band detected any clouds in the estuary mouth, those images were excluded from the analysis. Because the two cloud filters assessed different aspects of the imagery—metadata and potential clouds within the study areas—the double filter excluded more cloudy images from analysis compared to if we had used only one cloud filter.

After applying both cloud filters, we then calculated the Normalized Difference Water Index (NDWI, Eq. 1) for the Sentinel-2 MSI imagery (McFeeters, 1996). NDWI is commonly used in remote sensing of water extent (Ashok et al., 2021; Heimhuber et al., 2021; Roca et al., 2022). Each pixel of the image was assigned an NDWI value, and this index was used to detect water pixels from non-water pixels.

$$NDWI = \frac{R_{rs}(559) - R_{rs}(864)}{R_{rs}(559) + R_{rs}(864)} \quad (1)$$

In Eq. 1, $R_{rs}(559)$ represents reflectance values at 559 nm and refers to the green band, while $R_{rs}(864)$ represents reflectance values at 864 nm and refers to the near-infrared (NIR) band. On a scale of approximately −0.8 to 0.8, low negative values indicate vegetation, values near 0 indicate non-vegetated areas, and high positive values indicate water. In an effort to create a water/non-water binary, we investigated setting an NDWI threshold of 0.0, 0.05, and 0.10. Based on a visual examination

of the output binary from these different thresholds, we selected an optimal threshold and included it in the CEA tool, based on which one produced the highest accuracy for the estuary mouth state analysis when compared to visual inspection. After generating the water/non-water binary, we filtered out small vestigial clusters of less than 100 pixels—clusters likely due to waves and rocks. We then used an object-based analysis to determine if the estuary mouth was open (i.e., water pixels were connected from the interior of the estuary to the ocean) or closed (i.e., water pixels were not connected). If water pixels were connected, the tool would detect a single object and return a value of 1. If the water pixels were not connected, the tool would detect two objects and return a value of 2.

Inundation

We conducted an inundation analysis in GEE on the two sites, Russian River and Navarro, with the highest mouth detection accuracy compared to visual inspection (see the "Estuary Mouth State Accuracy" section). First, the inundation shapefile was used to calculate the total area of inundation. Next, two methods were used to calculate inundation extent: one using Sentinel-2 MSI imagery (Fig. 2B) and one using Sentinel-1 C-SAR imagery (Fig. 2C). For the approach using Sentinel-2 MSI imagery, we applied the same two cloud filters used for the estuary mouth state analysis and calculated NDWI to generate a water/non-binary image using the same threshold as was selected for that site from the estuary mouth state analysis.

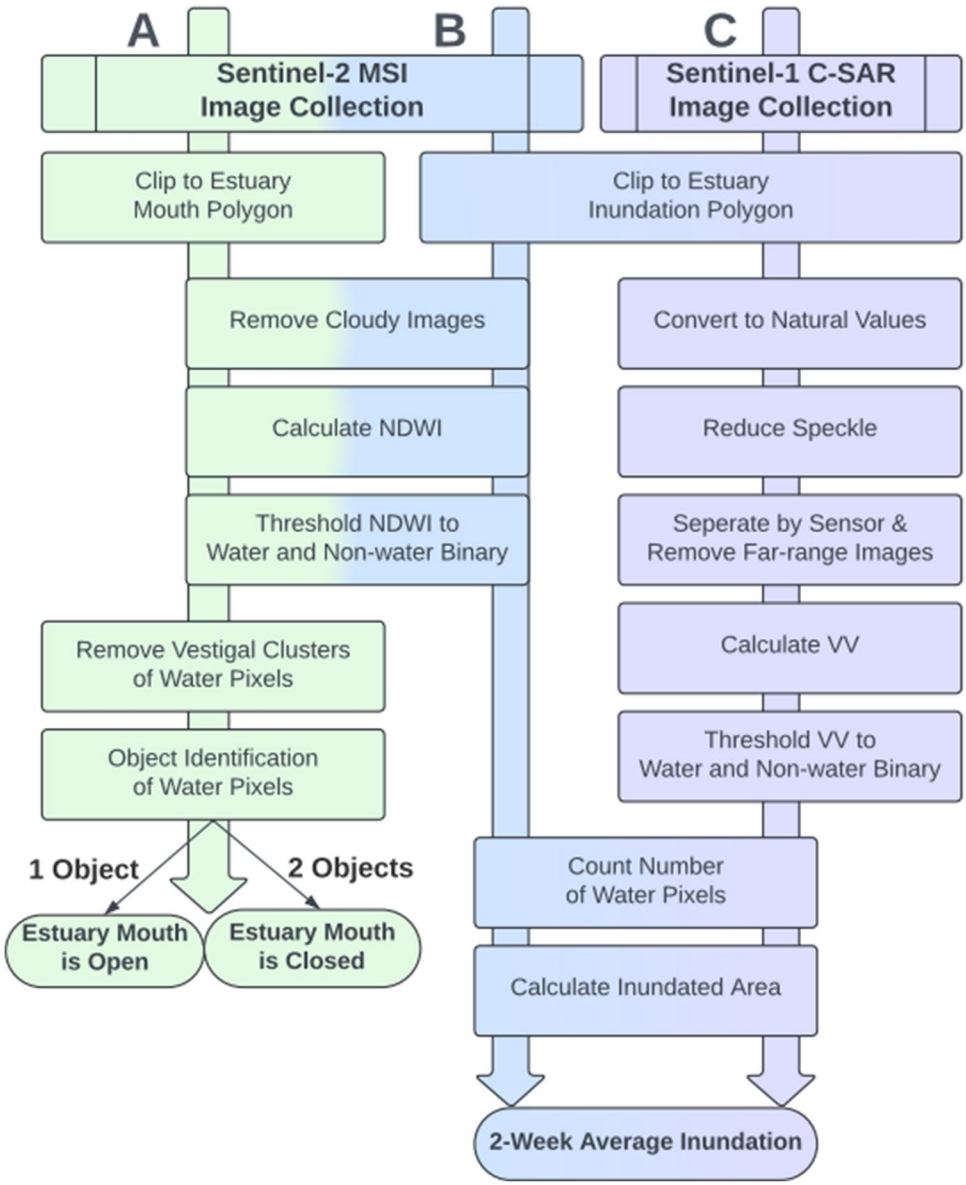

Fig. 2 The California Estuary Assessment Tool workflow to determine estuary mouth state and inundation extent. The green arrow (**A**) represents the Sentinel-2 MSI processing to determine the estuary mouth state. The blue arrow (**B**) represents the Sentinel-2 MSI processing to calculate the inundation extent. The purple arrow (**C**) represents the Sentinel-1 C-SAR processing to calculate the inundation extent

For the second inundation extent approach, we used Sentinel-1 C-SAR imagery. In order to prepare the Sentinel-1 C-SAR imagery for analysis, we applied multiple preprocessing techniques. First, we converted the data from decibels (dB) to natural values. Next, we employed the Refined Lee Filter technique to reduce speckle, a phenomenon present in SAR data where non-target backscatter distorts image interpretation. The Refined Lee Filter is a recognized and respected speckle reduction technique that "select[s] similar pixels to reinforce homogeneity according to eight non-square windows as the templates" (Xing et al., 2017).

Having reduced speckle, we filtered the imagery by sensor and incidence angle. We first separated Sentinel-1 C-SAR imagery by satellite (Sentinel-1A and Sentinel-1B) due to minor calibration differences between each sensor (Schmidt et al., 2020) and then separated the imagery into near- or far-range bands based on the location of the study site within the area covered by the sensor. A study site in the near-range is closer to the sensor, and a study site in the far-range is farther from the sensor. We used the incidence angle to determine the location of the study site within the area covered by the sensor. An angle between 36° and 40° was selected as the midpoint to separate near and far-range.

After accounting for differences in the sensor and incidence angle, we determined with visual inspection that the VV (vertical transmit, vertical receive) polarization band in the near-range was the most successful at discerning sand from water at estuary mouths compared to the far-range and both iterations of the VH (vertical transmit, horizontal receive) polarization band. Based on these differences in polarization, the CEA tool filtered out any image in the far-range and only ran an analysis on near-range imagery in the VV band. This substantially reduced the number of images in the image collection, thereby reducing temporal resolution, but increased our confidence in the accuracy of the results. From Navarro, 145 far-range images were removed from a total of 354 images for our study period, and for Russian River, 79 far-range images were removed from a total of 212 images. Similar to thresholding the Sentinel-2 MSI imagery based on NDWI values, we applied a threshold of 0.02 to the Sentinel-1B C-SAR imagery and a threshold of 0.025 to the Sentinel-1A C-SAR imagery in order to distinguish water pixels from non-water pixels. We selected these thresholds after iterating through a range of threshold values across several study sites and several dates as a means of discerning which threshold performed best at identifying estuary features compared to true color Sentinel-2 MSI imagery. Different thresholds were selected for Sentinel-1A C-SAR and Sentinel-1B C-SAR due to the minor calibration differences mentioned above. Having completed preprocessing, we generated a water/non-water binary using the respective thresholds for each sensor and interleaved the data from the two different sensors into a single time series.

After creating image collections where all pixels are distinguished into binary classes of water/non-water for both Sentinel-2 MSI and Sentinel-1 C-SAR, we determined the total number of water pixels per image. We multiplied this number by 100 (Sentinel-2 MSI and Sentinel-1 C-SAR have a resolution of 10 m by 10 m per pixel) to get the area of water in square meters. We then created a time series using a running 2-week average for the area values obtained from Sentinel-2 MSI and Sentinel-1 C-SAR to reduce noise and generate a smoother single-time series visualization (henceforth referred to as the combined running average). We chose this window as it balanced smoothing out noise while also capturing the rapid inundation changes characteristic of this size of bar-built estuaries.

Accuracy Assessment

To determine the accuracy of the CEA tool's estuary mouth state analysis and inundation extent, we used a number of cross comparisons which we detail in the following paragraphs. For the estuary mouth state, we compared the CEA tool to visual inspection of high-resolution satellite imagery, to another remotely sensed tool called InletTracker, and to inundation extent. For inundation extent, we compared both outputs from Sentinel-1 C-SAR and Sentinel-2 MSI to each other and then we compared their combined running average to in situ water level data and its derived hypsometric inundation extent.

To determine the accuracy of the CEA tool's estuary mouth state analysis, we visually inspected imagery. Visual inspection of imagery, especially of high spatial resolution imagery, such as that of PlanetScope, is an established method to assess the accuracy of water masks produced by coarser spatial resolution satellite imagery (Mukherjee et al., 2024; Su et al., 2024). Every available Sentinel-2 MSI image was recorded in one of four categories: open mouth state, closed mouth state, cloudy, or uncertain. We designated an image as uncertain when the mouth state was difficult to discern due to the imagery's resolution of 10 m. We further investigated Sentinel-2 MSI images that were deemed uncertain by comparing them to higher resolution 3 m PlanetScope imagery taken on the same day. If a Planet image on the same date was available, the researchers changed the uncertain designation to open or closed based on visual inspection of higher-resolution imagery. If PlanetScope imagery was not available, we left the designation as uncertain.

In addition to validating the CEA tool's mouth state detection by visually inspecting imagery, we compared these results to InletTracker. InletTracker is an open-source, GEE-enabled Python software package that uses Landsat 5, 7, and 8 and Sentinel-2 MSI imagery to determine if an inlet is open or closed. Specifically, InletTracker uses least-cost analysis to infer whether an estuary inlet is open or closed (Heimhuber et al., 2021). This tool first uses CoastSat, a custom GEE-enabled Python package, to sharpen images

and remove cloudy pixels. InletTracker then takes the images processed in CoastSat and applies a least-cost pathfinding approach. The least-cost pathfinding approach places a different weight on water and non-water pixels and keeps track of the pixel values along the estuary berm (following the shoreline) and the path of pixels across the estuary berm (connecting the interior to the exterior of the estuary). It evaluates the paths along and across the estuary berm to determine if there is a large difference where the paths intersect (suggesting an open estuary) or if there is a small difference (suggesting a closed estuary; Heimhuber et al., 2021). We ran InletTracker with recommended metrics: a minimum of ten open and ten closed designations for training data, NIR for pathfinding, and NDWI for analyzing the difference between along and across berm paths.

Sentinel-2 MSI and Sentinel-1 C-SAR water/non-water classes were also compared to one another on days when there was available imagery from both sensors to assess differences between the two inundation extent outputs. When the CEA tool indicated an image had a very low inundation level that was below what could be reasonably expected, that image was removed from the analysis. Often, these images were cloudy and should have initially been excluded.

Additionally, in situ water level data was used in conjunction with DEMs to derive inundation extent from a hypsometric curve that was used to validate remotely sensed inundation extent. First, we matched remotely sensed observations with in situ observations by generating timestamps of imagery in the GEE time series and timestamps of in situ data (in UTC time) and matching the data. Data were matched as closely as possible with in situ data for the time of image capture. We generated hypsometric curves based on NOAA CoNED 1 m DEM. Hypsometric curves are graphical representations of the area at different elevations. In an estuary or water body, they illustrate the extent of inundated areas at different water levels. To validate the CEA tool's inundation extent, we used Pearson's correlation tests to compare the three CEA tool–generated inundation products to in situ water level data as well as inundation extent derived from hypsometric curves.

Finally, we compared remotely sensed inundation to remotely sensed mouth state. We visually inspected changes in inundation extent that occurred following changes in mouth state. Then, we calculated median changes in relative inundation extent (compared to the closest previous image) associated with the relative mouth state. Here, relative mouth state is defined as the relationship between detected estuary mouth states of two sequential images within a 7-day period. The four relative mouth states are "closed to open," "stayed open," "open to closed," and "stayed closed." In other words, we assessed if the CEA tool captured expected changes in inundation extent associated with changes in mouth state.

Seasonality

To evaluate seasonal patterns of estuary mouth state and inundation extent, we divided our time series into meteorological seasons. For estuary mouth state, we used Pearson's chi-squared test to assess seasonal differences in the distribution of instances of detected mouth states. For inundation, we calculated the median relative inundation values for each inundation metric (inundation extent and relative values of inundation for each sensor and the combined running average) by season, where relative inundation is defined as the inundation relative to the maximum verified inundation during the study period. Additionally, we assessed the variability of a 2-week average of Sentinel-1 C-SAR and Sentinel-2 MSI-derived inundation values (measured by variance) by season and tested the homogeneity of variances between seasons using Levene's test and a Bonferroni correction. This inundation product was selected for further analysis because it smoothed noise and artifacts in images and it correlated reasonably well with in situ data compared to Sentinel-1 C-SAR and Sentinel-2 MSI (see "Inundation Accuracy" section).

Results

Estuary Mouth State Accuracy

The CEA tool's cloud filter accuracy ranged from 70 to 84% compared to a visual inspection of the entire Sentinel-2 MSI image collection. The CEA tool's cloud filter is often overfiltered—that is, it skipped images in the collection that were actually cloud-free. Comparing the CEA tool cloud filter to InletTracker's, we found that InletTracker's cloud filter was more accurate, ranging from 88 to 91% across the five study sites. However, while the CEA tool's reduced number of images decreased the temporal resolution of the estuary mouth state analysis time series, it increased the detection accuracy. Therefore, we made no changes to the CEA tool to increase the number of frames.

In addition to the cloud filter, the NDWI threshold proved critical for the success of the CEA tool's estuary mouth state analysis. Previous studies have used a threshold of 0.1 to extract water from Sentinel-2 MSI-derived NDWI images (Kaplan & Avdan, 2017). In comparison, we found that different NDWI thresholds for each site increased the accuracy of estuary mouth state analysis: 0.1 for Russian River and Malibu; 0.05 for Navarro and Ventura; and 0.0 for Carmel.

The accuracy of the CEA tool's estuary mouth state analysis compared to visual inspection of the imagery also varied among sites. Russian River had the highest accuracy at 84% (Table 2). Other estuaries varied in accuracy with Navarro

Table 2 Accuracy of the CEA tool and InletTracker's cloud filter and estuary mouth state analysis when compared to visual inspection of the Sentinel-2 MSI collection for each estuary

	Accuracy of cloud filter compared to visual inspection		Accuracy of mouth analysis compared to visual inspection		CEA and InletTracker Agree
	CEA Tool	InletTracker	CEA Tool	InletTracker	
Navarro	88%	89%	80%	52%	60%
Russian	82%	91%	84%	44%	57%
Carmel	70%	89%	75%	70%	66%
Malibu	81%	91%	70%	68%	75%
Ventura	84%	88%	60%	24%	29%

at 80%, Carmel at 75%, Malibu at 70%, and Ventura at 60% (Table 2).

In a comparison of the CEA tool estuary mouth state analysis to that of InletTracker, we found that the CEA tool outperformed InletTracker at our five study sites. InletTracker's accuracy was 52% at Navarro, 44% at Russian, 70% at Carmel, 68% at Malibu, and 24% at Ventura (Table 2, Supplementary Information Tables 1 and 2). InletTracker ran on more images because its cloud filter did not filter out as many images as the CEA tool, giving InletTracker a higher temporal resolution but a lower accuracy due to cloud obstruction. Because of this, the CEA tool provides fewer observations within a given time period, and may miss some instances of mouth closure and opening, but provides a higher accuracy compared to InletTracker.

Inundation Accuracy

At Russian River, Sentinel-1 C-SAR-derived inundation extent correlated more strongly with in situ water level data and hypsometric curve data (Pearson's correlation, $R^2 = 0.23$ and $R^2 = 0.24$, respectively) than Sentinel-2 MSI-derived inundation extent did (Pearson's correlation, $R^2 = 0.07$ and $R^2 = 0.07$, respectively). At Navarro, however, Sentinel-1 C-SAR-derived inundation extent correlated weakly with in situ water level data and hypsometric curve data (Pearson's correlation, $R^2 = 0.06$ and $R^2 = 0.07$, respectively), as did Sentinel-2 MSI-derived inundation extent (Pearson's correlation, $R^2 = 0.14$ and $R^2 = 0.01$) (Figs. 3A and 4A). Compared to individual sensor measurements of inundation, the 2-week average of Sentinel-1 C-SAR and Sentinel-2 MSI

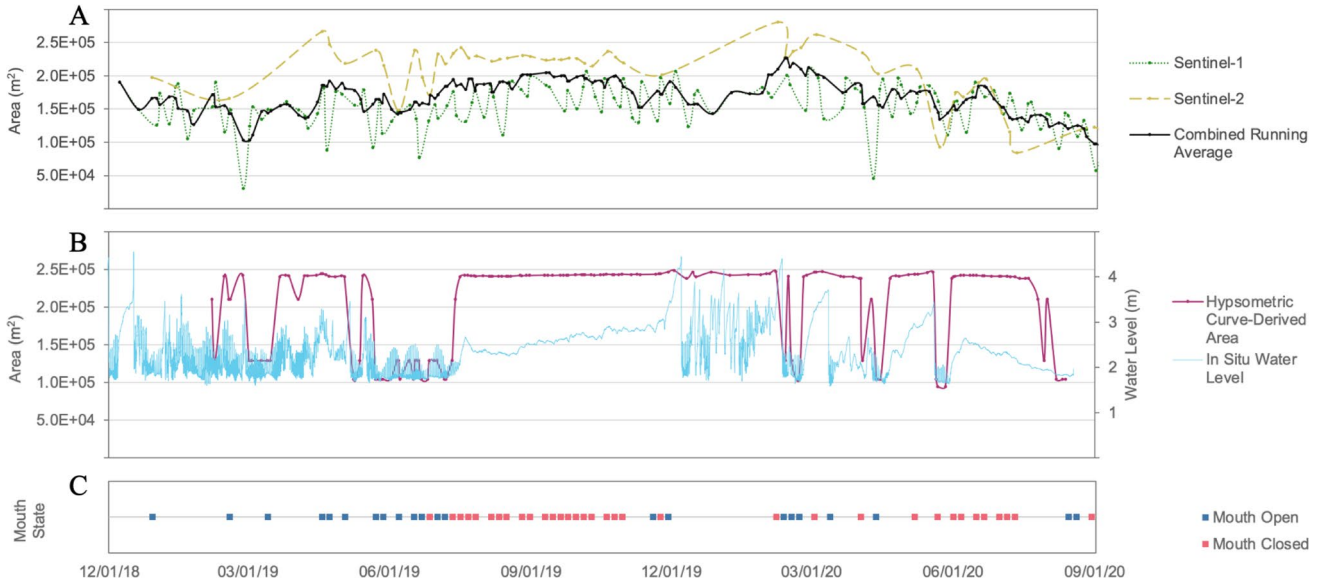

Fig. 3 Inundation extent, water level, and mouth state at the Navarro River Estuary from December 2018 to September 2020. **A** The CEA tool's satellite-derived inundation extent for Sentinel-1 C-SAR in green, Sentinel-2 MSI in yellow, and their combined 2-week running average in black. **B** In situ water level data is in blue and hypsometric curve-derived area in pink. **C** CEA tool's estuary mouth state with an open mouth state is in blue and a closed mouth state in red

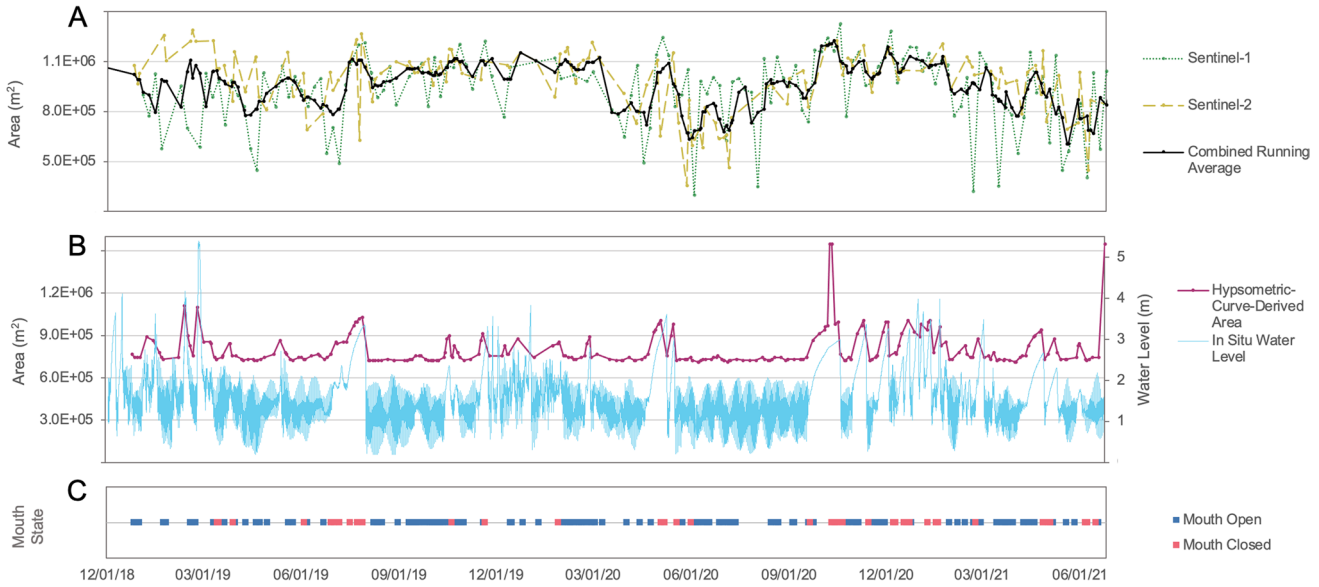

Fig. 4 Inundation extent, water level, and mouth state at Russian River Estuary from December 2018 to July 2021. **A** The CEA tool's satellite-derived inundation extent for Sentinel-1 C-SAR in green, Sentinel-2 MSI in yellow, and their combined 2-week running average in black. **B** In situ water level data is in blue and hypsometric curve derived area in pink. **C** CEA tool's estuary mouth state with an open mouth state is in blue and a closed mouth state in red

observations generally correlated more closely than individual sensors (with the exception of Sentinel-1 C-SAR at Russian River) with in situ water level data at Russian River (Pearson's correlation, $R^2 = 0.21$) and Navarro (Pearson's correlation, $R^2 = 0.17$). Compared to in situ data, the combined running average observations correlated substantially less closely with hypsometric curve data ($R^2 = 0.06$ at Russian River, $R^2 = 0.10$ at Navarro River). In situ and hypsometric curve data were positively correlated more strongly at Russian River ($R^2 = 0.98$) than at Navarro River ($R^2 = 0.51$) (Figs. 3B and 4B).

Sentinel-1 C-SAR-derived inundation extent exhibited more variability in the time series compared to that of Sentinel-2 MSI. Although Sentinel-1 C-SAR and Sentinel-2 MSI results differed from each other, the time series of both exhibited similar dips and peaks at each site that correlated with available water level data (Figs. 3B and 4B). In situ data indicates a modest increase in water level in December 2019 at Navarro River. Satellite images in the period December 2019 through February 2020 are scarce, but after this data gap, satellite data indicate a modest increase in March 2020. The satellite data then indicate decreases in water level beginning in approximately June 2020 that continued until approximately September 2020, which aligned with in situ water level data.

Mouth State and Inundation Relationship Accuracy

We identified instances in which the CEA tool detected mouth state change accurately and associated inundation change successfully (Figs. 3C and 4C). Overall, both satellite sensors detected decreases in inundation extent following mouth state opening ("closed to open" state, Table 3),

Table 3 Median change in inundation extent for each relative mouth state by estuary for Sentinel-1 C-SAR (S1), Sentinel-2 MSI (S2), and the combined 2-week running average of Sentinel-2 MSI and Sentinel-1 C-SAR (S1 and S2)

	Navarro			Russian		
	S1	S2	S1 and S2	S1	S2	S1 and S2
Closed to open	− 16.5% ($n = 2$)	− 18.7% ($n = 3$)	+ 5.7% ($n = 4$)	− 8.4% ($n = 1$)	− 1.6% ($n = 12$)	0.0% ($n = 12$)
Stayed open	*NA* ($n = 0$)	− 7.0% ($n = 6$)	+ 3.6% ($n = 6$)	− 14.5% ($n = 11$)	− 0.4% ($n = 63$)	0.0% ($n = 64$)
Open to closed	+ 13.5 ($n = 1$)	− 0.4% ($n = 4$)	+ 3.7% ($n = 4$)	*NA* ($n = 0$)	+ 4.3% ($n = 6$)	+ 0.3% ($n = 6$)
Stayed closed	+ 15.5% ($n = 8$)	− 0.5% ($n = 28$)	0.0% ($n = 28$)	+ 13.3% ($n = 4$)	− 1.5% ($n = 16$)	+ 1.2% ($n = 16$)

Sample sizes of inundation measurements derived from Sentinel-2 MSI are larger than those derived from Sentinel-1 C-SAR because they more often align with the Sentinel-2 MSI-derived mouth state observation

with the exception of the combined running average. Larger changes in inundation extent were detected at the Navarro River Estuary for this relative mouth state compared to those detected at the Russian River Estuary. For instance, at the Navarro River Estuary, the changes in inundation following a change in mouth state are clearly visible (Figs. 5 and 6). In this case, the mouth changed from closed on February 7, 2020, to open on February 12, 2020. Using visual inspection of true color imagery and comparison to in situ and hypsometric data, we determined that this change was indeed followed by a decrease in inundation. In this specific case, however, only Sentinel-2 MSI detected a decrease in inundation (18.7%). In contrast, Sentinel-1 C-SAR incorrectly detected a 30.6% increase in inundation, likely due to the sensor incorrectly identifying wet sand as water, thereby overestimating inundation extent.

For the "open to closed" relative mouth state, the CEA tool accurately detected increases in inundation extent associated with mouth closure for Sentinel-2 MSI and the combined running average at Russian River and Sentinel-1 C-SAR and the combined running average at Navarro River (Table 3). Although there were not enough Sentinel-1 C-SAR images at Russian River to calculate median change due to far-range images being filtered out and Sentinel-2 MSI images at Navarro River incorrectly calculated a slight decrease in inundation, visual inspection reveals that the imagery overall captures the expected outcome. For example, at the Russian River Estuary, the mouth state changed from open on November 19, 2019, to closed on November 21, 2019 (Figs. 7 and 8). Both Sentinel-1 C-SAR and Sentinel-2 MSI detected increases in inundation following this event, with increases in inundation of 23.4% and 11.1% for each satellite sensor, respectively. Further, these observations align with in situ water level data, indicating a steady increase in water level as the water presumably pools behind the bar within the estuary (Fig. 4).

For the "stayed open" relative mouth state, individual satellite sensors detected a slight decrease in inundation at both sites. For the "stayed closed" relative mouth state, satellite sensors indicated increases in inundation at both sites using Sentinel-1 C-SAR imagery. There was a slight decrease detected with Sentinel-2 MSI (Table 3). Overall, Sentinel-1 C-SAR imagery captured greater changes in inundation extent compared to changes captured by Sentinel-2 MSI. The combined running average of both sensors deviated from individual sensor measurements for most mouth states.

Seasonal Patterns

Navarro River and Russian River exhibited very different patterns of mouth state overall, as well as differing seasonal patterns. Navarro River had a much higher proportion of closed to open mouth state observations compared to Russian River such that the proportions were nearly inverted (Fig. 9). While 30% of 83 Navarro mouth state observations were of open mouth state, 26% of Russian River's 146 mouth state observations were of a closed mouth state. At Navarro River, a closed mouth state was most frequently observed in fall, followed by spring. The ratio of mouth state observations in fall differed significantly from spring and winter ($p < 0.05$). An open mouth state was most frequently observed in spring followed by winter. At Russian River, in contrast, an open mouth state was most frequently observed in fall, followed closely by winter, spring, and summer. Closed mouth state was detected fairly evenly across seasons, although summer had slightly more closed mouth state observations

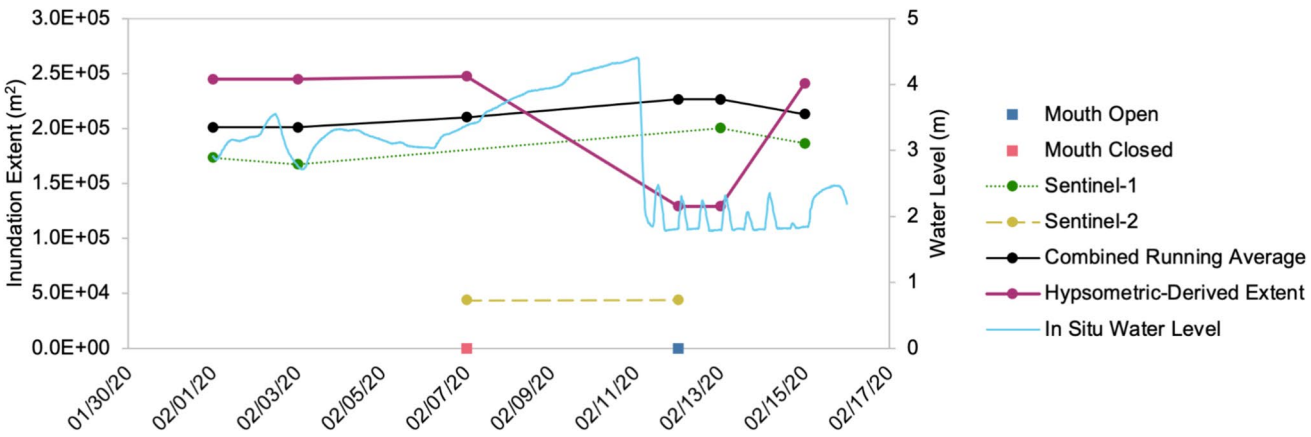

Fig. 5 A comparison of the CEA tool's mouth state, CEA tool's inundation extent, in situ water level data, and hypsometric inundation extent at Navarro River Estuary. The CEA tool detected a closed mouth state on February 7, 2020 (red square), and an open mouth state on February 12, 2020 (blue square). The CEA tool's satellite-derived inundation extent for Sentinel-1 C-SAR is in green, Sentinel-2 MSI in yellow, and their combined 2-week running average in black. In situ water level data is in blue and hypsometric inundation extent in pink

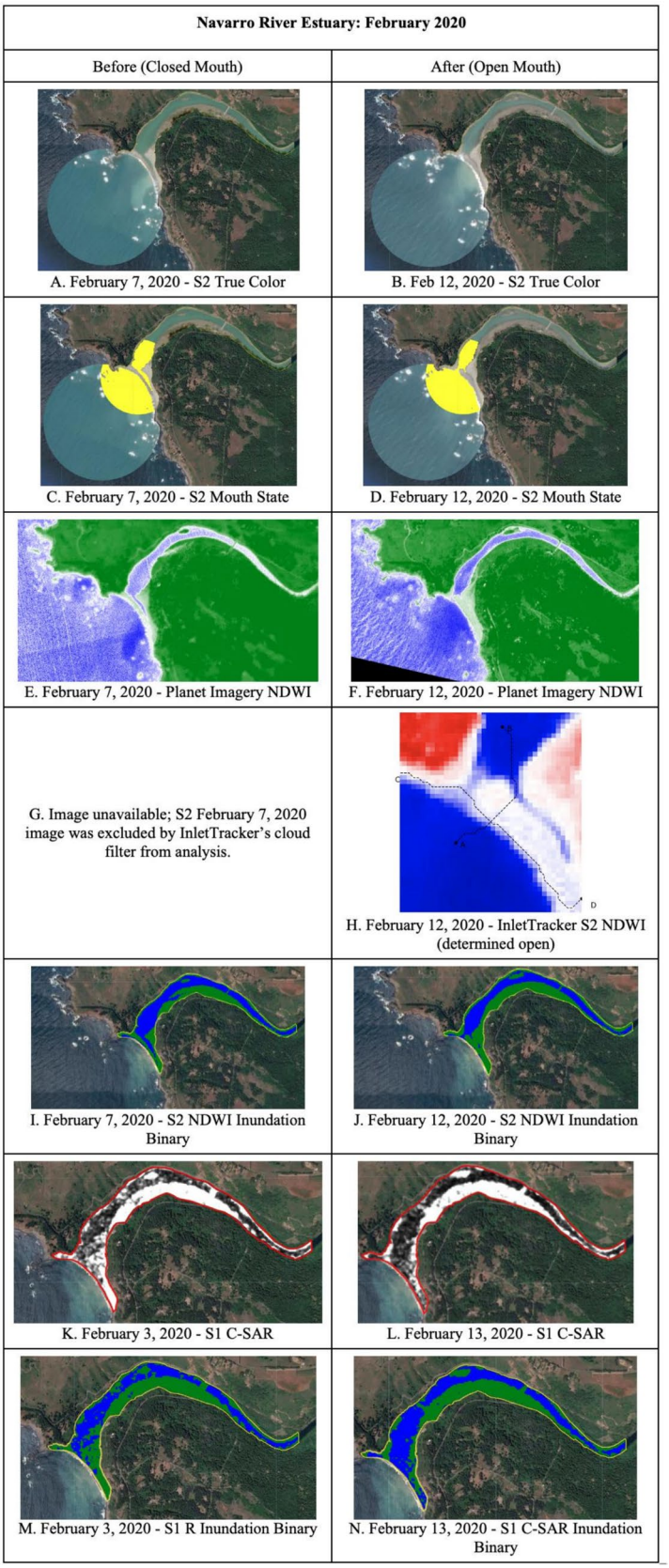

Fig. 6 Navarro River Estuary change in mouth state from closed (February 7, 2020) (left column) to open (February 12, 2020) (right column) and associated inundation extent changes. **A**, **B** Sentinel-2 MSI (S2) true color imagery; **C**, **D** mouth state layer determining a single object or two objects; **E**, **F** PlanetScope Normalized Difference Water Index (NDWI); **G**, **H** InletTracker S2 NDWI; **I**, **J** S2 NDWI inundation binary; **K**, **L** Sentinel-1 C-Synthetic Aperture Radar (S1 C-SAR) backscatter; **M**, **N** S1 C-SAR inundation binary

than other seasons. The ratio of mouth state observations did not differ significantly between seasons.

When comparing the median inundation extent by season, both estuaries and satellite sensors diverged from each other (Table 4, Fig. 10). In all seasons except summer at both estuaries, Sentinel-2 MSI detected higher inundation extents compared to Sentinel-1 C-SAR. At Navarro River, the lowest median inundation extent detected by the combined running average occurred in summer, whereas the highest occurred in winter (Fig. 10A). At Russian River, the lowest median inundation extent detected by the combined running average occurred in summer whereas the highest occurred in fall (Fig. 10B).

Variability of inundation values varied widely between seasons and between estuaries. At Navarro River, fall exhibited significantly higher variance than all other seasons (Fig. 10A) (winter and spring, $p < 0.001$; summer, $p < 0.01$). Summer had the second highest variance, which differed significantly from spring ($p < 0.01$). Spring exhibited the least variability, followed by winter. In contrast, variability at Russian River was highest for summer and spring (Fig. 10B). The variance of summer values was significantly higher than fall ($p < 0.001$) and winter ($p < 0.01$), and the variance of spring values was significantly higher than fall ($p < 0.01$) and winter ($p < 0.05$).

Discussion

Accuracy

The CEA tool determined the estuary mouth state with high accuracy compared to visual inspection. Past studies have used multi-source, remotely sensed data to monitor wetland ecosystems (Guo et al., 2017), detect nearshore bars (Román-Rivera & Ellis, 2019), and even assess inundation over time (Eid et al., 2020). However, our literature review yielded only one major alternative methodology for detecting the estuary mouth state, which was the InletTracker tool (Heimhuber et al., 2021). As noted in Table 2, InletTracker was more successful at filtering clouds compared to the CEA tool; however, the CEA tool was more accurate at detecting estuary mouth state at large estuaries. Due to differences in filtering clouds, the CEA tool ran on fewer images than InletTracker. InletTracker uses CoastSat, which has additional functions for image preprocessing and creates a more robust cloud filter. This led the CEA tool to have a lower temporal resolution because more images were excluded from the analysis. Furthermore, images with clouds were more frequently able to surpass the CEA cloud filter, sometimes resulting in an incorrect classification of the estuary mouth state.

The CEA tool had higher accuracy compared to InletTracker for the sites examined because of its unique method for detecting the estuary mouth state. The CEA tool uses an object-based approach while InletTracker uses a least-cost pathfinding approach. The BBE study sites for the CEA tool often had narrow sandbars closing off the estuary with variable and sometimes distant breach locations north or south of the primary inlet opening. Given InletTracker's least-cost pathfinding approach, the specific characteristics of these estuaries sometimes resulted in InletTracker misidentifying the narrowest part of sandbar as a breach. In such instances, the CEA tool had higher accuracy for the sites examined. However, InletTracker has the capacity to be refined by changing the type of analysis and conducting a visual inspection before producing results. For the sake of comparing methodologies, these adjustments to InletTracker were not investigated but could increase the tool's accuracy. InletTracker and the CEA tool complement one another by

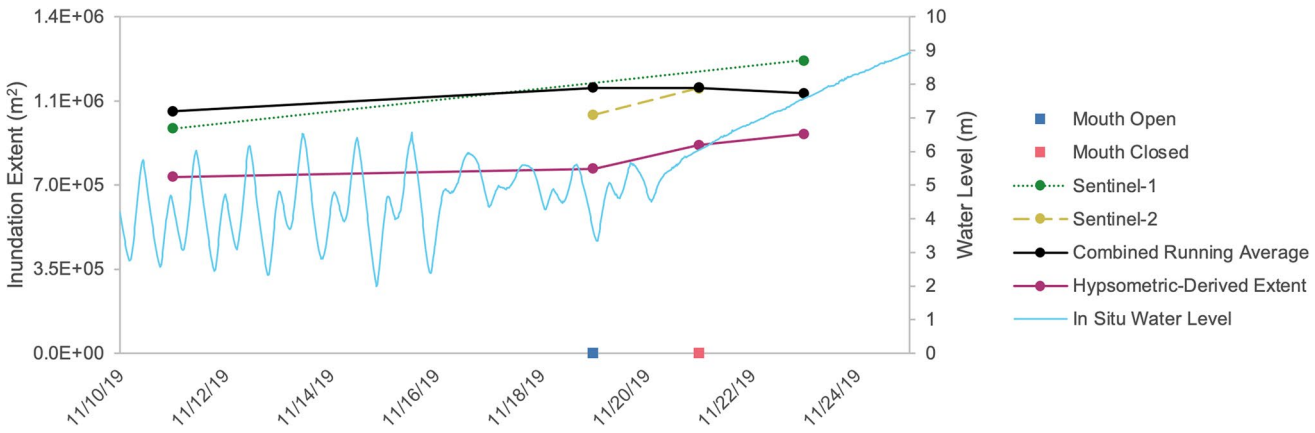

Fig. 7 A comparison of the CEA tool's mouth state, CEA tool's inundation extent, in situ water level data, and hypsometric inundation extent at the Russian River Estuary. The CEA tool detected an open mouth state on November 19, 2019 (blue square), and a closed mouth state on November 21, 2019 (red square). The CEA tool's satellite-derived inundation extent for Sentinel-1 C-SAR is in green, Sentinel-2 MSI in yellow, and their combined 2-week running average in black. In situ water level data is in blue and hypsometric inundation extent in pink

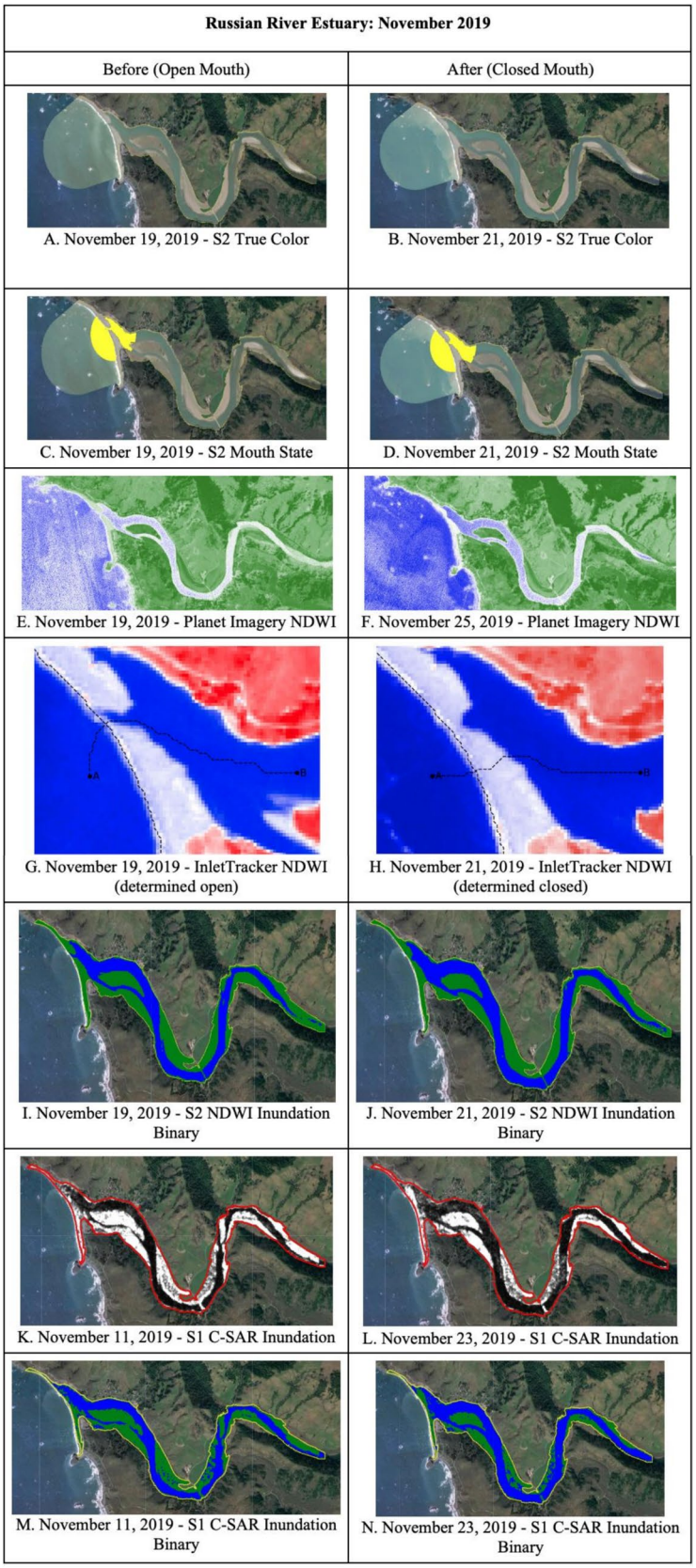

Fig. 8 Russian River Estuary change in mouth state from open (November 19, 2019) (left column) to closed (November 21, 2019) (right column) and associated inundation extent changes. **A**, **B** Sentinel-2 MSI (S2) true color imagery; **C**, **D** mouth state layer determining a single object or two objects; **E**, **F** PlanetScope Normalized Difference Water Index (NDWI); **G**, **H** InletTracker S2 NDWI; **I**, **J** S2 NDWI inundation binary; **K**, **L** Sentinel-1 C-SAR (S1 C-SAR) backscatter; **M**, **N** S1 C-SAR inundation binary

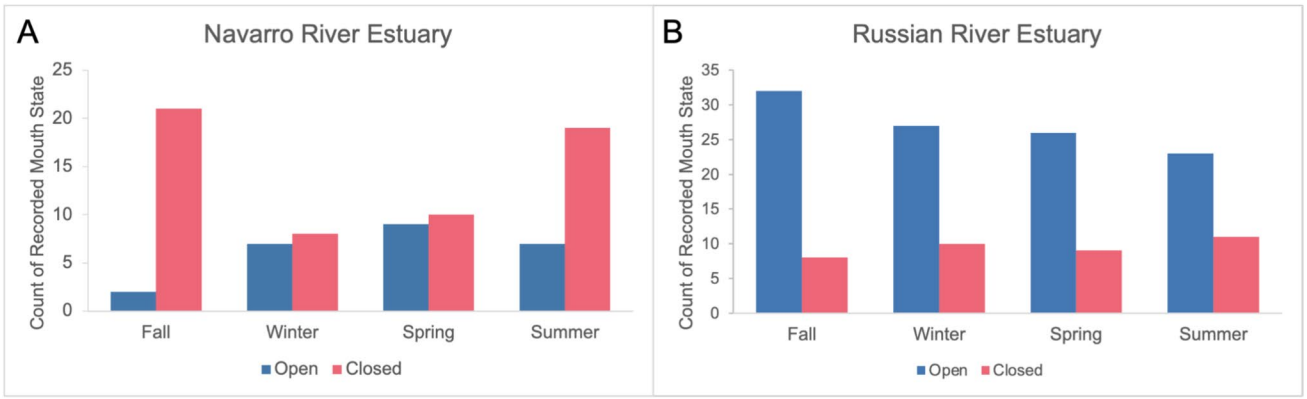

Fig. 9 Observations of open estuary mouth states in blue and closed estuary mouth states in red for **A** Navarro River Estuary and **B** Russian River Estuary

Table 4 Median relative inundation values for each season by estuary for Sentinel-1 C-SAR (S1), Sentinel-2 MSI (S2), and their combined 2-week running average (S1 and S2)

	Navarro			Russian		
	S1	S2	S1 and S2	S1	S2	S1 and S2
Fall	71.7% ($n = 42$)	76.6% ($n = 19$)	73.2% ($n = 55$)	81.1% ($n = 27$)	82.6% ($n = 39$)	86.2% ($n = 58$)
Winter	80.3% ($n = 50$)	82.2% ($n = 15$)	75.8% ($n = 63$)	75.5% ($n = 28$)	85.4% ($n = 35$)	85.8% ($n = 60$)
Spring	75.0% ($n = 65$)	79.1% ($n = 16$)	73.0% ($n = 78$)	67.3% ($n = 42$)	77.5% ($n = 35$)	74.6% ($n = 74$)
Summer	73.5% ($n = 58$)	69.9% ($n = 26$)	71.5% ($n = 82$)	70.8% ($n = 40$)	65.4% ($n = 36$)	68.3% ($n = 72$)

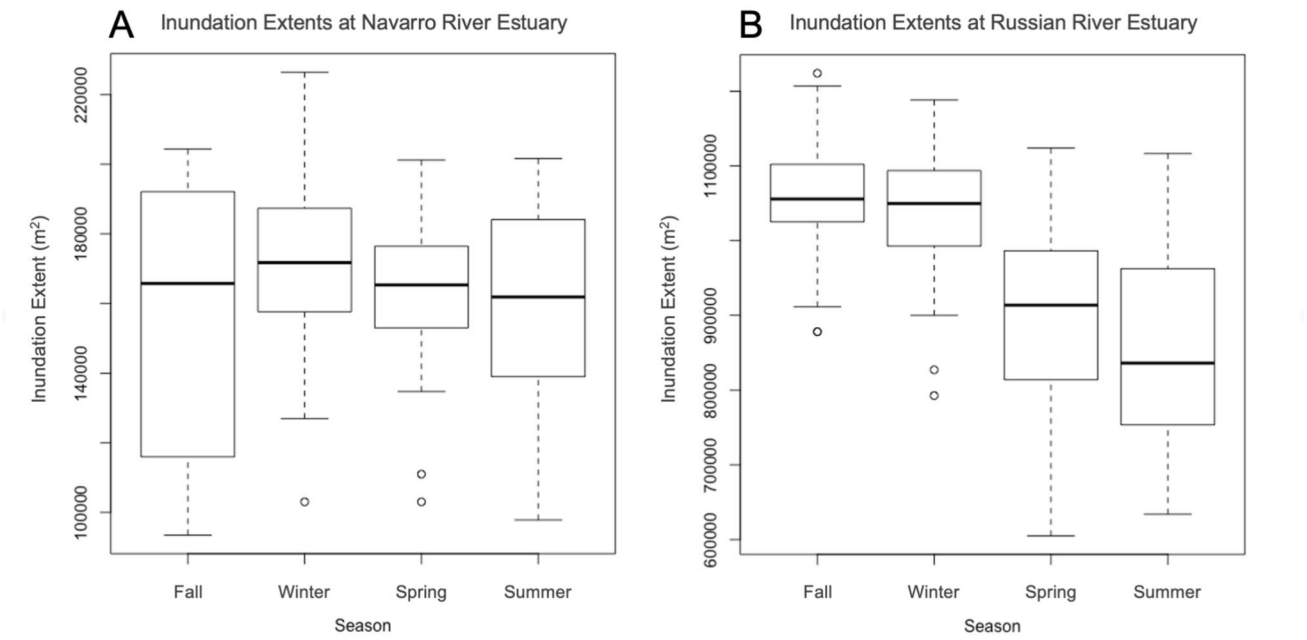

Fig. 10 Distribution of inundation extent values for the combined 2-week running average of Sentinel-1 C-SAR and Sentinel-2 MSI by season at **A** Navarro River Estuary and **B** Russian River Estuary

providing different methodological approaches to investigate changes in estuary mouth state over time.

Satellite-derived inundation extent was corroborated by in situ data. Satellite-derived inundation extents from both sensors had consistent trends. Upon visual inspection of the imagery, Sentinel-2 MSI inundation was most accurate when sun glint or algae did not interfere with the spectral signature of the water, and Sentinel-1 C-SAR was most accurate when the water surface was smoother. Overall, Sentinel-1 C-SAR correlated more strongly with in situ water level data than Sentinel-2 MSI. Neither sensor correlated particularly highly with in situ water level, likely because the relationship between inundation and water level varies from site to site and is not expected to be linear. These findings are consistent with the established literature (Largier et al., 2019). Inundation extent also did not correlate highly with hypsometric curve data. This is likely due to errors in using satellite imagery to estimate inundation extent and due to morphological change. For this reason, the benefit of using hypsometric data was determined to be limited in this case study. Despite this, CEA tool-derived inundation metrics such as relative inundation extent or change in inundation may in the future be used in conjunction with other measures, such as last visible mouth state observation, to provide more nuanced and higher resolution predictions of estuary mouth state (e.g., by using an inferential model).

Median change in inundation extent by relative mouth state (Table 3) in many instances aligns with the in situ water level data for these two sites as well as previous research characterizing bar-built estuaries (Clark & O'Connor, 2019). A BBE mouth often opens from a closed state following an increase in fluvial inputs and wave overtopping events, increasing water levels and inundation extents. Therefore, a breach event results in lower water levels inside the BBE compared to the previous closed mouth state. Sentinel-1 C-SAR and Sentinel-2 MSI both detected decreases in inundation following a mouth opening. However, the combined running average of the two sensors did not detect decreases. This may be because increasing inundation extents leading up to a breach result in a positive mean. The increases in inundation level for "stayed closed" state, as detected by Sentinel-1 C-SAR, also concur with existing research on BBEs, as water levels rise as they continue to receive fluvial inputs. This further suggests that both sites did not experience substantial beach berm seepage and instead slowly filled during their closed states. Similarly, a change from an open to closed mouth state would be likely associated with an increase in inundation extent as captured by the CEA tool in this study. The CEA tool diverges from the literature for the "stayed open" relative mouth state. In situ inundation extent changes in a "stayed open" condition are often more variable due to daily fluctuations associated with ocean tides (Bertin & Olabarrieta, 2016), whereas the CEA tool suggests a decrease in inundation extent at both sites for this relative mouth state. The combined running average appears to not capture sudden changes in inundation extent as well as single-sensor observations do, but it may be better suited for assessing longer-term changes in inundation extent over time (for example, seasonally).

Seasonality

The proportion of open mouth state observations was highest in spring and followed by winter at Navarro River (Fig. 9A), while at Russian River, it was highest in fall followed by winter (Fig. 9B). This differs slightly from our hypothesis that open mouth state observations would be highest in winter and early spring. This can be due to differing timing or effect of river discharge or wave action in each of these BBEs. Further, our inundation extent variability results did not align with our hypothesis that inundation extent would be more variable in winter and spring. Instead, inundation extent variability was more closely tied to the frequency of mouth closure, which is further discussed below. Our findings at both BBEs contradicted our original hypothesis that summer would exhibit the least changes in mouth state and inundation extent (Figs. 9 and 10).

Navarro River and Russian River varied in mouth state and inundation extent patterns (Figs. 9 and 10). At Navarro, the higher the ratio of closed to open mouth state observations, the more variance in inundation extent. For example, in the fall, the ratio of closed to open mouth state observations is the highest (21:2) and inundation variability is the highest. This holds true for all seasons. In other words, inundation extent (and presumably water level) varies more as the mouth closes more frequently and/or stays closed for longer periods. This aligns with in situ water level data for the period (Fig. 3B) which reveals steady increases in water level (and presumably pooling) in summer 2019 and steady decreases in water level (presumably seepage) during summer 2020, suggesting frequent and/or long mouth closures in both periods.

At Russian River, the ratio of closed to open mouth state does not correspond as neatly to the variability of inundation as it does at Navarro River. However, the number of closed mouth state observations appears to correspond slightly to increasing variability of inundation extent in each season (Fig. 9 and 10B). For example, the CEA tool collected the highest number of closed mouth state observations in summer, which is when inundation extent was most variable. This aligns with the in situ water level at Russian River, which demonstrates high water level variability (and presumably inundation extent variability), particularly in summer 2019 (Fig. 4B).

Although the CEA tool cannot characterize closed mouth state with certainty (i.e., distinguish between a closure after a

brief, undetected opening versus a consistently closed mouth state), a higher number of closed mouth state observations can be interpreted as more frequent and/or longer mouth closures. At both estuaries, increased variability in inundation extent is associated with more frequent/longer mouth closures. At Navarro River, this variability occurs primarily in fall, followed by summer. At Russian River, however, this variability occurs primarily in summer, followed by spring. Previous literature has found that BBE water level fluctuates most in spring and late fall due to fluvial discharge and wave overtopping events, respectively (Clark & O'Connor, 2019). Russian River deviates notably from these findings, perhaps because Clark and O'Conner (2019) summarize patterns of BBEs, from which Russian River deviates. Other previous research on historical closure records for Russian River finds that most closures occur in October to November (Behrens et al., 2013), from which our findings also differ. This may be because closed mouth state observations do not necessarily equate to the number of closures or because our time period differs from that of Behrens et al. (2013).

Observed differences between Navarro River and Russian River may be largely explained by management strategies. Russian River is heavily managed, with 80% of breaches since the 1960s conducted by public agencies (Behrens et al., 2013). This may explain why the season of largest inundation extent (winter) corresponds with the season with the most open mouth state observations—breaches here are frequently conducted for flood management purposes, resulting in artificial breaching when water levels are high (Largier et al., 2019). This may also explain why the seasons with the highest median inundation values (fall and winter) have the least amount of variability.

Application and Limitations

Previously, a lack of data on breaching has limited the validation of modeling efforts (such as those of Behrens et al., 2013) on California BBEs. The CEA tool may be used to validate this model at other sites beyond the Russian River. Behrens et al. (2013) also note a lack of coincident years of available data to assess the relationship between the ENSO events or Pacific Decadal Oscillation cycles and mouth closure. By offering a retrospective view of closure events and associated trends in inundation, the CEA tool may contribute to filling that gap and providing enough data to complement modeling efforts where they were previously data-limited. Improved modeling efforts may then be used to forecast closures in the future, thereby improving the management of estuarine systems.

While the CEA tool successfully assesses breach state and inundation, it is not without limitations. The primary source of error in the estuary mouth state analysis was incorrectly interpreting an open mouth state as closed (Supplementary Information Tables 1 and 2). Often, a perched mouth state with a small stream connecting the estuary interior to the ocean (i.e., Ventura and Carmel River Estuaries) was not captured by the CEA tool. Rather, we found the tool would more often correctly identify full breaches with wide streams (i.e., Russian and Navarro River Estuaries). The most probable reason for this is that the 10 m spatial resolution of the imagery did not detect smaller streams. Another limitation of the CEA tool is that it can only capture one image every few days, while an estuary may fully open and close within a day. Additionally, the differing spectral resolutions of Sentinel-2 MSI and Sentinel-1 C-SAR may impact our results for breach identification and inundation. As a multispectral passive sensor, Sentinel-2 MSI uses rather broad sections of reflected or emitted light for multiple wavelengths to identify water—specifically, the reflected green wavelength represented at 559 nm and near-infrared wavelength represented at 864 nm. In contrast, the active sensor of Sentinel-1 C-SAR has a VV response from a single wavelength (5.405 GHz) that is based on the physical properties (geometry and electromagnetic properties) of the target. Because each sensor relies on different physical properties to identify water, their results may not align in both mouth state and inundation. This distinction is observed in the misidentification of pixels as water or non-water for the inundation assessments. Sentinel-1 C-SAR frequently misidentified sandbar pixels as water and Sentinel-2 MSI frequently misidentified pixels obscured by sun glint and algae. In many instances, the Sentinel-2 MSI underestimated the inundation extent, and conversely, Sentinel-1 C-SAR overestimated the inundation extent by misidentifying sand pixels as water. Additionally, the Sentinel-1 C-SAR output sometimes misidentified rougher surface waters as land due to the more diffuse backscatter they project. Similar to the estuary mouth state analysis, the small size of these estuaries most likely meant that the spatial resolution of the Sentinel-2 MSI and Sentinel-1 C-SAR products was too coarse to effectively detect the true area of inundation for each estuary. However, the high accuracy of the estuary mouth state detection and consistency of inundation detection from both sensors indicate that, with an understanding of limitations, the CEA tool is accurate enough to use.

Potential further improvements in the CEA tool include new methodologies and an expansion of the tool's geographic and functional scope. The tool's cloud filter could be updated to increase the temporal resolution and accuracy of the optical imagery. One potential revision to the methodology for Sentinel-1 C-SAR preprocessing techniques entails comparing and enhancing data preparation with the work of Mullissa et al. (2021), which showcases a more thorough methodology for using Sentinel-1 C-SAR in GEE. Another Sentinel-1 C-SAR methodology improvement involves utilizing Sentinel-2 MSI imagery to systematically correct

for Sentinel-1 C-SAR's limitations. Further exploration of supervised classification is also recommended for identifying water/non-water areas. Possible expansions of the tool include refining the currently measured water quality metrics like sea surface temperature and turbidity analysis and adding new water quality metrics, such as submerged aquatic vegetation, colored dissolved organic matter, chlorophyll-a, and transmissivity. Testing the tool at other sites would increase the applicability and capacity of the tool.

Conclusions

The multiple habitats and high biodiversity characteristic of BBEs are in large part due to varying water levels resulting in variable inundation extents, as different habitats are suited to differing periods and frequency of inundation (Behrens et al., 2013). Of particular importance, however, are flooding frequency and duration, which are positively correlated with the health of BBEs (Largier et al., 2019; Clark & O'Connor, 2019). This study finds that closed mouth state is associated with variability of inundation extent and therefore variable marsh inundation. Further, we find substantial differences in patterns of mouth state and inundation between two BBEs—including nearly inverted ratios of open to closed mouth state observations and differing seasonal timing of peak inundation extent—highlighting the variability that exists between individual systems. Because flooding period is an important driver of estuary health (Clark & O'Connor, 2019) and breaching too frequently at low water levels can permanently change habitats and estuary condition (Largier et al., 2019), the historical record of inundation extent and mouth state is critical for long-term planning and management of BBEs.

A better understanding of the frequency, seasonality, and duration of mouth closure is critical for estuary management. With the CEA tool, estuary managers will be able to better analyze patterns of estuary mouth closure and inundation extent, informing key management decisions such as the timing of managed breaches, frequency of dredging, and sediment management. Compared to other tools to monitor estuaries, including InletTracker, the CEA tool is unique in providing a graphical user interface that does not require coding knowledge, making it potentially more accessible for estuary practitioners. Estuary managers can use the tool to examine breaches from late 2018 to the present day as GEE continually updates its image collections, allowing for retrospective and near real-time analysis. Furthermore, managers of BBEs beyond our study sites will be able to apply this tool for their own management purposes by simply creating and uploading shapefiles for their own BBEs of interest.

The CEA tool is, at the time of writing, still pending public release. Our Supplemental Information includes the ReadMe of the CEA Tool explaining the different functions and parameters needed to run the tool. Once the code is cleared through NASA's software release, it will be available for public use at the NASA DEVELOP GitHub: https://github.com/NASA-DEVELOP/. It will also be hosted on the USC Sea Grant website here: https://dornsife.usc.edu/uscseagrant/climate-change-and-coastal-studies/.

Supplementary Information The online version contains supplementary material available at https://doi.org/10.1007/s12237-025-01545-w.

Acknowledgements The NASA DEVELOP Coastal California Water Resources II group would like to thank our project partners and contributors including Michael Esgro at the Ocean Protection Council; Dr. Eric Stein and Kris Taniguchi-Quan at the Southern California Water Research Project; Ross Clark and Kevin O'Connor at Moss Landing Marine Laboratories Central Coast Wetlands Group; Dr. Kyle Cavanaugh at the University of California, Los Angeles; Dr. John Largier at the University of California, Davis; and The Bay Foundation. Their field perspective, expertise, and encouragement were essential to ensure the CEA tool could be utilized for improved wetland monitoring and management. This research was carried out in part at the Jet Propulsion Laboratory, California Institute of Technology, under contract with the National Aeronautics and Space Administration. SP, KA, MB, RD, AG, RL, SS, and EC were supported by DEVELOP as part of NASA's Applied Sciences Program. The CEA tool code will become publicly available on the NASA DEVELOP GitHub: https://github.com/nasa-develop. NASA's Technical Reports Server hosts the DEVELOP project's final presentation and is available here: https://ntrs.nasa.gov/citations/20210019621.

Funding This material is based upon work supported by NASA through contract NNL16 AA05 C.

Declarations

Competing Interests The authors declare no competing interests.

References

Ashok, A., Rani, H. P., & Jayakumar, K. V. (2021). Monitoring of dynamic wetland changes using NDVI and NDWI based landsat imagery. *Remote Sensing Applications: Society and Environment, 23*, 100547. https://doi.org/10.1016/j.rsase.2021.100547

Barbier, E. B., Georgiou, I. Y., Enchelmeyer, B., & Reed, D. J. (2013). The value of wetlands in protecting southeast Louisiana from hurricane storm surges. *PLoS ONE, 8*(3), e58715.

Behrens, D. K., Bombardelli, F. A., Largier, J. L., & Twohy, E. (2009). Characterization of time and spatial scales of a migrating river-mouth. *Geophysical Research Letters, 36*, L09402. https://doi.org/10.1029/2008GL037025

Behrens, D. K., Bombardelli, F. A., Largier, J. L., & Twohy, E. (2013). Episodic closure of the tidal inlet at the mouth of the Russian River—A small bar-built estuary in California. *Geomorphology, 189*, 66–80.

Bertin, X., Mendes, D., Martins, K., Fortunato, A. B., & Lavaud, L. (2019). The closure of a shallow tidal inlet promoted by infragravity waves. *Geophysical Research Letters, 46*(12), 6804–6810.

Bertin, X., & Olabarrieta, M. (2016). Relevance of infragravity waves in a wave-dominated inlet. *Journal of Geophysical Research: Oceans, 121*(8), 5418–5435.

Clark, R., Clark, C., Heady, W., O'Connor, K., Ryan, S., Stoner-Duncan, S. (2013). Using new methodologies to assess bar-built estuaries along California's coastline. Final Report. *US Environmental Protection agency (Region 9)*, award no. CD-00T20101.

Clark, R., & O'Connor, K. (2019). A systematic survey of bar-built estuaries along the California coast. *Estuarine, Coastal and Shelf Science, 226*, 106285.

Coastal National Elevation Database (CoNED). (n.d.). Project - Topobathymetric Digital Elevation Model (TBDEM) Digital Object Identifier (DOI) number: /https://doi.org/10.5066/F7Z60MHJ

Copernicus Sentinel-1 C-SAR Level 1 Data. [2014–2021]. (n.d.). Retrieved from Google Earth Engine, processed by ESA.

Copernicus Sentinel-2 MSI Level-2A Data [2017–2021]. (n.d.). Retrieved from Google Earth Engine, processed by ESA. https://doi.org/10.5066/F76W992G

Dahl, T. E. (1990). Wetlands losses in the United States, 1780's to 1980's. *US Department of the Interior, Fish and Wildlife Service*.

Dawson, J., Orescanin, M. M., Clark, R., & O'Connor, K. (2023). Spatiotemporal variability of dissolved oxygen in response to morphological state in a central California coast bar-built estuary. *Estuarine, Coastal and Shelf Science, 282*, 108241.

Eid, A. N. M., Olatubara, C. O., Ewemoje, T. A., El-Hennawy, M. T., & Farouk, H. (2020). Inland wetland time-series digital change detection based on SAVI and NDWI indices: Wadi El-Rayan lakes. *Egypt. Remote Sensing Applications: Society and Environment, 19*, 100347.

Elachi, C., & van Zyl, J. (2006). *Introduction to the physics and techniques of remote sensing*. Wiley.

Gonenc, A., Ozerdem, M.S. & Emrullah, A.C.A.R. (2019). Comparison of NDVI and RVI vegetation indices using satellite images. In *2019 8th International Conference on Agro-Geoinformatics (Agro-Geoinformatics)* (pp. 1–4). IEEE.

Goodwin, P. & Cuffe, K. (1994). Russian River estuary study: Hydrologic aspects of an estuary management plan. *Technical Report for Sonoma County Dept. of Planning, City, CA* (194 pp.).

Gorelick, N., Hancher, M., Dixon, M., Ilyushchenko, S., Thau, D., & Moore, R. (2017). Google earth engine: Planetary-scale geospatial analysis for everyone. *Remote Sensing of Environment*, *202*, 18–27. https://doi.org/10.1016/j.rse.2017.06.031

Guo, M., Li, J., Sheng, C., Xu, J., & Wu, L. (2017). A review of wetland remote sensing. *Sensors, 17*(4), 777.

Harris, P. T., Heap, A. D., Bryce, S. M., Porter-Smith, R., Ryan, D. A., & Heggie, D. T. (2002). Classification of Australian clastic coastal depositional environments based upon a quantitative analysis of wave, tidal, and river power. *Journal of Sedimentary Research, 72*(6), 858–870.

Heady, W. N., Clark, R. P., O'Connor, K., Clark, C., Endris, C., Ryan, S., & Stoner-Duncan, S. (2015). Assessing California's bar-built estuaries using the California Rapid Assessment Method. *Ecological Indicators, 58*, 300–310.

Heimhuber, V., Vos, K., Fu, W., & Glamore, W. (2021). InletTracker: An open-source Python toolkit for historic and near real-time monitoring of coastal inlets from Landsat and Sentinel-2. *Geomorphology, 389*, 107830.

Kaplan, G., & Avdan, U. (2017). Object-based water body extraction model using Sentinel-2 satellite imagery. *European Journal of Remote Sensing, 50*(1), 137–143.

Kirlin, J., Caldwell, M., Gleason, M., Weber, M., Ugoretz, J., Fox, E., & Miller-Henson, M. (2013). California's Marine Life Protection Act Initiative: Supporting implementation of legislation establishing a statewide network of marine protected areas. *Ocean & Coastal Management, 74*, 3–13.

Largier, J., O'Connor, K. & Clark, R. (2019). *Considerations for management of the mouth state of California's bar-built estuaries*. Final Report (NA14NMF437012).

McFeeters, S. K. (1996). The use of the Normalized Difference Water Index (NDWI) in the delineation of open water features. *International Journal of Remote Sensing, 17*(7), 1425–1432. https://doi.org/10.1080/01431169608948714

Mukherjee, R., Policelli, F., Wang, R., Arellano-Thompson, E., Tellman, B., Sharma, P., Zhang, Z., & Giezendanner, J. (2024). A globally sampled high-resolution hand-labeled validation dataset for evaluating surface water extent maps. *Earth System Science Data, 16*(9), 4311–4323. https://doi.org/10.5194/essd-16-4311-2024

Mullissa, A., Vollrath, A., Odongo-Braun, C., Slagter, B., Balling, J., Gou, Y., Gorelick, N., & Reiche, J. (2021). Sentinel-1 SAR backscatter analysis ready data preparation in Google Earth Engine. *Remote Sensing, 13*(10), 1954.

Orescanin, M. M., Coughlin, J., & Young, W. R. (2021). Morphological response of variable river discharge and wave forcing at a bar-built estuary. *Estuarine, Coastal and Shelf Science, 258*, 107438.

Orescanin, M. M., & Scooler, J. (2018). Observations of episodic breaching and closure at an ephemeral river. *Continental Shelf Research, 166*, 77–82.

Planet Team (2017). Planet application program interface: In space for life on Earth. San Francisco, CA. https://api.planet.com.

Ranasinghe, R., & Pattiaratchi, C. (2003). The seasonal closure of tidal inlets: Causes and effects. *Coastal Engineering Journal, 45*(4), 601–627. https://doi.org/10.1142/S0578563403000919

Rich, A., & Keller, E. A. (2013). A hydrologic and geomorphic model of estuary breaching and closure. *Geomorphology, 191*, 64–74.

Roca, M., Navarro, G., García-Sanabria, J., & Caballero, I. (2022). Monitoring sand spit variability using Sentinel-2 and Google Earth Engine in a Mediterranean estuary. *Remote Sensing, 14*(10), 2345. https://doi.org/10.3390/rs14102345

Román-Rivera, M. A., & Ellis, J. T. (2019). A synthetic review of remote sensing applications to detect nearshore bars. *Marine Geology, 408*, 144–153.

Schmidt, K., Schwerdt, M., Miranda, N., & Reimann, J. (2020). Radiometric comparison within the Sentinel-1 SAR constellation over a wide backscatter range. *Remote Sensing, 12*(5), 854.

Stretch, D., & Parkinson, M. (2006). The breaching of sand barriers at perched, temporary open/closed estuaries — A model study. *Coastal Engineering Journal, 48*(1), 13–30. https://doi.org/10.1142/S0578563406001295

Su, Z., Xiang, L., Steffen, H., Jia, L., Deng, F., Wang, W., Hu, K., Guo, J., Nong, A., Cui, H., & Gao, P. (2024). A new and robust index for water body extraction from Sentinel-2 imagery. *Remote Sensing*, *16*(15), Article 15. https://doi.org/10.3390/rs16152749

Thorne, K. M., Buffington, K. J., Jones, S. F., & Largier, J. L. (2021). Wetlands in intermittently closed estuaries can build elevations to outpace sea-level rise. *Estuarine, Coastal and Shelf Science, 257*, 107386. https://doi.org/10.1016/j.ecss.2021.107386

U.S. Fish & Wildlife Service (2018). *National wetlands inventory*. U.S. Fish & Wildlife Service. https://data.nal.usda.gov/dataset/national-wetlands-inventory.

U.S. Geological Survey, (2019). 3D Elevation Program 1-Meter Resolution Digital Elevation Model (published 20200606). Accessed 3 Jan 2019 at https://www.usgs.gov/the-national-map-data-delivery

Xing, X., Chen, Q., Yang, S., & Liu, X. (2017). Feature-based nonlocal polarimetric SAR filtering. *Remote Sensing, 9*(10), 1043.

Xu, H. (2006). Modification of normalised difference water index (NDWI) to enhance open water features in remotely sensed imagery. *International Journal of Remote Sensing, 27*(14), 3025–3033.